 doi:10.20944/preprints202201.0139.v1

Article

Quantitative optical coherence tomography for longitudinal monitoring of postnatal retinal development

Guangying Ma[1], Jie Ding[1], Tae-Hoon Kim[1], and Xincheng Yao[1,2,*]

[1] University of Illinois at Chicago, Department of Biomedical Engineering, Chicago, Illinois, United States
[2] University of Illinois at Chicago, Department of Ophthalmology and Visual Sciences, Chicago, Illinois, United States
* Correspondence: xcy@uic.edu

Featured Application: Quantitative optical coherence tomography (OCT) promises a noninvasive method for longitudinal monitoring of postnatal retinal development.

Abstract: A better study of the postnatal retinal development is not only essential for the in-depth understanding of the nature of the vision system but also may provide insights for treatment developments of eye conditions, such as retinopathy of premature (ROP). To date, quantitative analysis of postnatal retinal development is primarily limited to end-point histological examination. This study is to validate in vivo optical coherence tomography (OCT) for longitudinal monitoring of postnatal retinal development in developing mouse eyes. Three-dimensional (3D) frame registration and super averaging were adopted to investigate the fine structure of the retina. Interestingly, a hyporeflective layer (HRL) between the nerve fiber layer (NFL) and inner plexiform layer (IPL) was observed in developing eyes and gradually disappeared with aging. To interpret the observed retinal layer kinetics, a model based on eyeball expansion, cell apoptosis, and retinal structural modification was proposed.

Keywords: postnatal retinal development, retinal layer thickness, OCT

1. Introduction

The mammalian retina continuously grows after birth, which is so-called postnatal retinal development. Most of the cell differentiation, structure building, and synaptogenesis is complete at the time point of eye-opening [1]; while the retinal neurite circuit is still under development after eye-opening [2-4]. For mice, the dendrites of retinal ganglion cells (RGCs) ramify across the whole inner plexiform layer (IPL) at the time of birth and refine into different stratifications during postnatal retinal development [5]. After eye-opening, a light stimulation regulated RGCs dendritic lamination was observed. Around 40% bistratified RGC turned into monostratified [6,7]. With stratification refinement, the density of both ribbons and conventional synapses in the IPL continuously increases after eye-opening and reaches the peak level by around postnatal day (P) 21 [8]. However, the receptive field center size of RGCs of the mouse at P28 reduced from the mouse at P17 (3 days after eye-opening) [9]. All these studies indicated that the postnatal retinal development after the eye-opening is important to visual function. However, the study on developing mouse retinas is primarily limited to endpoint histological examination, which limits its dynamic observation of developing retinal architecture. Thus, *in vivo* imaging method for longitudinal monitoring of postnatal retinal development is desirable.

This study is to validate optical coherence tomography (OCT) for longitudinal monitoring of postnatal retinal development in developing mouse eyes. OCT has been widely

 doi:10.20944/preprints202201.0139.v1

used in ophthalmology clinics and research for its excellent depth-resolved capability [10]. For instance, the retinal thickness, as a reflection of total cell number and retinal structure complexity, has been used as a biomarker for retina degeneration [11-13], and damage recovery [14,15] studies. Retinal layer thickness abnormity has been also associated with retinopathy of premature (ROP). Compared with the normally developed retina, for ROP, the photoreceptor layer was thinner, and the inner nuclear layer (INL)was thicker [16]. As a new OCT modality, OCT angiography has been used to monitor vascular changes in normal developing and diseased animal models [17-19].

In this study, longitudinal OCT of developing mouse eye was conducted from the eye-opening, i.e., P14, up to P56. Mouse models have been extensively used for the study of normal retinal development and inherited retinal diseases [20,21]. Quantitative analysis of individual retinal layers was analyzed and discussed. Three-dimensional (3D) frame registration and super averaging [22-24] were adopted to investigate the fine structure of the retina. Interestingly, a hyporeflective layer (HRL) between the nerve fiber layer (NFL) and inner plexiform layer (IPL) was observed in developing eyes and gradually disappeared with aging. On the contrary, the IPL stratification structure was not clear at an early age but gradually developed with aging. To interpret the observed retinal layer development, a model based on eyeball expansion, cell apoptosis, and retinal structural modification is discussed.

2. Materials and Methods

2.1. Animal preparation

All animal care and experiments were conformed to the Association for Research in Vision and Ophthalmology statement for the use of animals in ophthalmic and vision research. All experiments were conducted following the protocols approved by the Animal Care Committee at the University of Illinois Chicago (UIC). C57BL/6J mice were grouped with P14, P17, P21, P28, P56. Each group contained 5 or 6 mice. The mice were housed in the Biology Resource Lab of UIC with 14-hour light and 10-hour dark circulation. Before OCT recording, the mice were anesthetized with a mixture of 100 mg/kg ketamine and 5mg/kg xylazine injected intraperitoneally. A heating pad was used to maintain body temperature during image recording. The pupil was fully dilated with 0.5% tropicamide. A cover glass, along with lubricant eye gel (GenTeal, Alcon Laboratories, Fort Worth, TX), was placed on the cornea to prevent drying as well as to serve as a contact concave lens to improve the image quality.

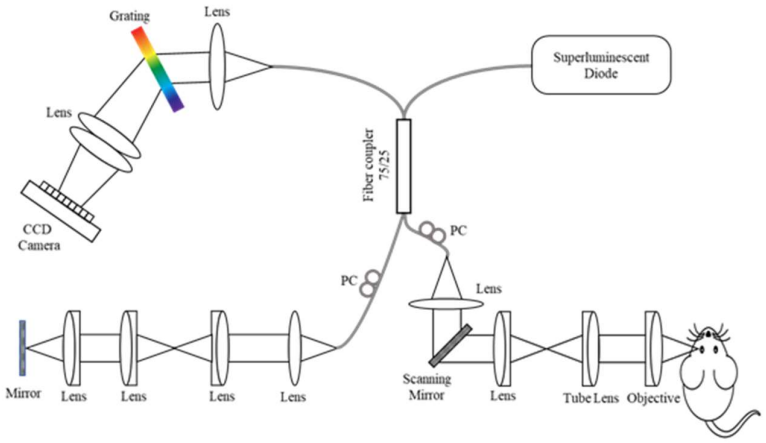

Figure. 1. The diagram of the custom-designed optical coherence tomography (OCT) system. PC, polarization controller.

2.2. Imaging system setup

Custom-designed OCT has been used for in vivo imaging study of mouse retina [25,26]. Figure 1 shows the schematic diagram of the system used for this study. A broadband (M-T-850-HP-I, Superlum, Cork, Ireland, $\lambda_{center} = 850\,nm, \Delta\lambda = 165\,nm$) superluminescent diode (SLD) was used as the light source. A fiber coupler (TW850R5A2, Thorlabs, USA; 75:25) divided the OCT light to the sample and reference arms. A custom-designed spectrometer was constructed with a line CCD camera (OCTOPLUS, e2v, Chelmsford, UK; 2048 pixels) and a transmission grating (Wasatch Photonics, West Logan, Utah; 1200 line/mm). The axial and lateral resolution of the system was theoretically estimated at 1.4 and 3 μm, respectively. The pixel resolution is 1.2 μm in both axial and lateral dimensions.

2.3. Data acquisition and image processing

For the retinal layer thickness measurement, 3D raster scan volume data was taken at the optic nerve head, nasal, dorsal, temporal, and ventral quadrants. For the retina layer thickness time course change measurement, the B-scan in the center location of a dorsal quadrant was measured. For the measurement of HRL thickness distribution, the retina was divided into 8 parts. In each part, the center B-scan was selected and segmented for HRL thickness measurement. For the retina inner layer structure analysis, the dorsal quadrant was imaged with a field of view as $600\,\mu m$ containing 500 A-scans and 500 B-scans. 200 repetitive 3D volumes were collected with an A-scan rate of 80 kHz. The total recording time was 13.5 min.

For image processing, the standard OCT image reconstruction and post-processing procedure were applied. Briefly, the workflow was k-sampling, interferogram extraction, apodization, fast Fourier transform (FFT), and image registration. Thereafter, the retinal layer thickness was manually measured using MATLAB. For inner retinal structure analysis, frame registration was applied [24]. Briefly, each OCT volume was considered as a rigid cubic, four degrees of freedom were registered to adjust the direction and location of the OCT volumes. The procedure was as follows, first, the *en face* image of each OCT volume was produced to get an image stack, then the stack was registered using a plugin function in ImageJ named MultiStackReg. During the registration, the transformation matrix was recorded. Second, the enface registration transformation matrix was applied to all the data sets in MATLAB. Third, an image stack with the center B-scans of each volume was extracted. The stack was then registered with MultiStackReg, and the transformation matrix was recorded. Fourth, the B-scan registration transformation matrix was applied to all the data sets as well. The 200 OCT volumes were averaged to get a clear OCT 3D image [22,24].

3. Results

Preprints (www.preprints.org) | NOT PEER-REVIEWED | Posted: 11 January 2022 doi:10.20944/preprints202201.0139.v1

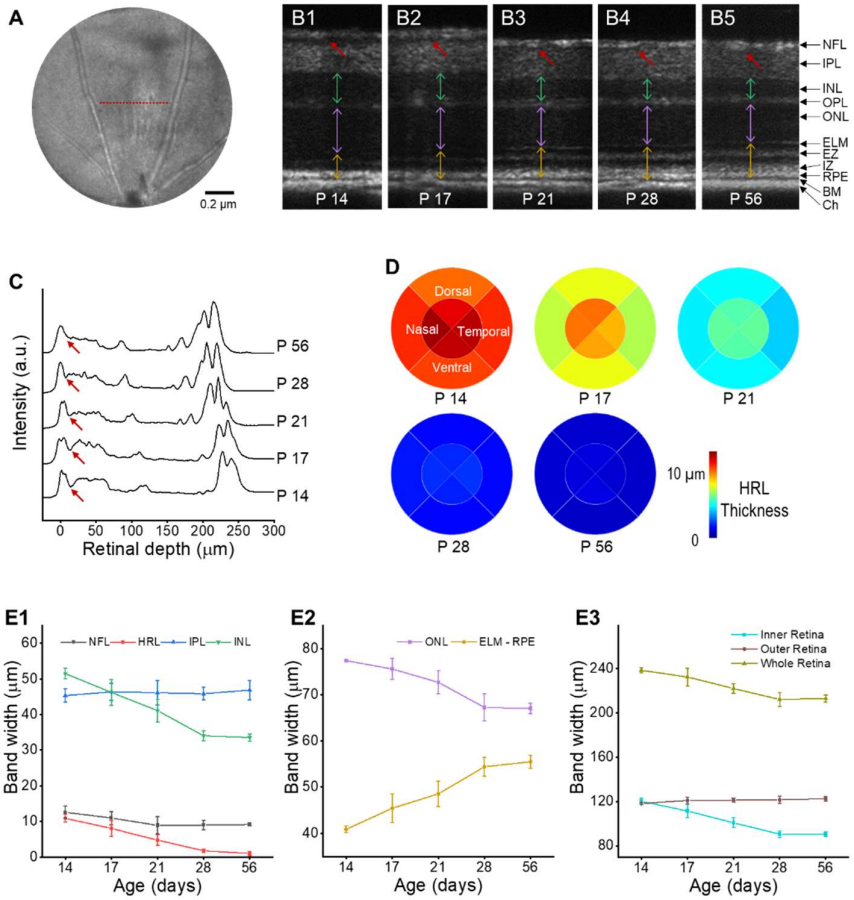

Figure. 2. Longitudinal OCT monitoring of developing retina. (A) Representative *en face* image of the dorsal quadrant of the mouse retina. The red line indicates the location for B-scan analysis. (B) Representative OCT B-scans of mouse retina from P14 to P56. The red arrows indicate the location of a hyporeflective layer (HRL). The green, purple, yellow two-head arrows indicate the thickness of INL, ONL, and ELM to RPE layers. (C) Line profiles of the image B-scans in B. The red arrows indicate the location of HRL. (D) Layer thickness changes of inner retina layers (D1), outer retina layers (D2), whole retina (D3). (E) The thickness distribution of HRL over time. The radius of the retina area is 1 mm. NFL, nerve fiber layer; HRL, hyporeflective layer; IPL, inner plexiform layer; INL, inner nuclear layer; ONL, outer nuclear layer; ELM, external limiting membrane; EZ, ellipsoid zone; IZ, interdigitation zone; RPE, retinal pigment epithelium; BM, Bruce membrane; Ch, choroid. In (D), each group was composed of 5-6 mice, and the error bars indicate the standard deviation.

Table 1. Quantitative thickness analysis of individual retinal layer changes with aging

Age	NFL (μm)	HRL (μm)	IPL (μm)	INL (μm)	ONL (μm)	ELM-RPE (μm)	Inner retina (μm)	Outer retina (μm)	Whole retina (μm)
P14	12.6 ± 1.7	10.9 ± 1.1	45.3 ± 1.9	51.5 ± 1.5	77.4 ± 0.3	40.9 ± 0.7	120.3 ± 2.5	118.3 ± 0.9	238.5 ± 2.3
P17	10.9 ± 1.8	8 ± 2.3	46.4 ± 2.4	46.2 ± 3.6	75.6 ± 2.2	45.4 ± 3.1	111.5 ± 6.2	121 ± 3	232.5 ± 8
P21	8.9 ± 2.4	4.7 ± 1.5	46.1 ± 3.5	41.1 ± 3.2	72.7 ± 2.5	48.6 ± 2.7	100.9 ± 4.4	121.3 ± 1.9	222.1 ± 4.4
P28	8.9 ± 1.3	1.7 ± 0.5	45.9 ± 1.8	34 ± 1.4	67.3 ± 2.9	54.4 ± 2	90.6 ± 3.1	121.7 ± 3.2	212.3 ± 6.2
P56	9.1 ± 0.5	1 ± 0.6	46.9 ± 2.7	33.6 ± 1	67 ± 1.1	55.5 ± 1.4	90.5 ± 2.2	122.6 ± 1.9	213.1 ± 3.2

 doi:10.20944/preprints202201.0139.v1

Figure 2 shows longitudinal OCT monitoring of developing retina, and the mean and standard deviation of layer thickness are summarized in Table 1. After eye-opening, the retinal layer thickness kept changing until P28. Figure 2A shows the *en face* image of the dorsal quadrant, which indicates the location of the B-scans in Figure 2B. Figure 2B shows the representative B-scans used for layer thickness measurement. The red arrows indicate an HRL which was unambiguously observed between P14 and P17, and gradually disappeared until P28. The green, purple, and orange two head arrows represent the thicknesses of the INL, outer nuclear layer (ONL), external limiting membrane (ELM) to retinal pigment epithelium (RPE). Figure 2C shows the reflectance profiles of the B-scans in Figure 2B, and the red arrows indicate the location of the HRL between NFL and IPL. Figure 2D shows the distribution of HRL thickness over the whole retina. The result shows that HRL existed all over the retina at P14 to P21, with the center region slightly thicker than the peripheral region. Figure 2E shows the layer thickness change with ages from P14 to P56. The inner retina layer thickness change is shown in Figure 2E1. The NFL thickness decreased from P14 to P21 and then remained the same. The HRL thickness kept decreasing after eye-opening and disappeared at about P28. The IPL thickness did not change significantly between P14 to P56 days. The INL thickness kept decreasing after eye-opening until P28. Figure 2E2 shows layer thickness change in the outer retina. The ONL thickness kept decreasing until P28. On the contrary, the ELM-RPE thickness kept increasing until P28. Figure 2E3 shows the thickness change of the inner retina, outer retina, and the whole retina. The thickness of the inner retina and the whole retina kept decreasing until P28. On the contrary, the thickness of the outer retina slightly increased after the eye-opening.

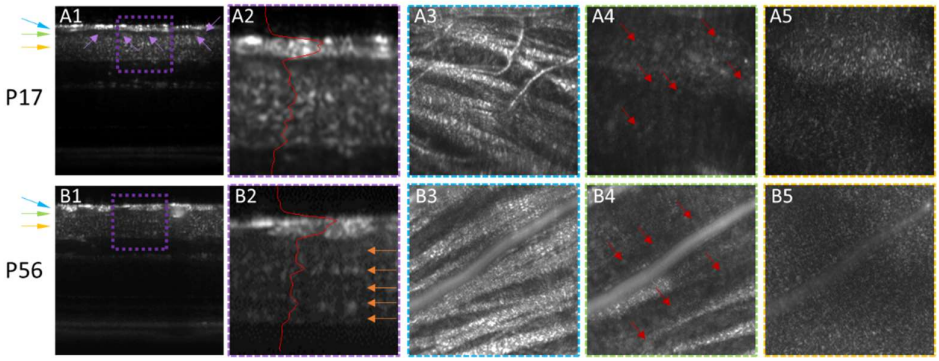

Figure 3. Comparative 3D OCT volumetric analysis of P17 (A) and P56 (B) mouse retinas. (A1, B1) Representative B-scans. The purple arrows in A1 indicate individual RGCs. (A2, B2) the enlarged view of the purple dash square in A1 and B1. The orange arrows in B2 indicate the stratification of IPL. (A3 to A5 and B3 to B5) are the en face images of NFL, GCL, and IPL, which corresponds to the location of the blue, green, and orange arrows in A1 and B1. The red arrows in A4 and B4 indicate the individual RGCs.

Figure 3 shows a comparative volumetric analysis of the inner retina of a P17 mouse (Figure 3A) and a P56 mouse. After frame registration and super averaging, the detailed structure was disclosed. In the OCT B-scan of the P17 mouse (Figure 3A1), individual RGCs were observed in the HRL. The stratification of the IPL of the P17 mouse was not clear; however, it was clearer for the P56 mouse (Figure 3A2 and B2). The nerve fibers of P17 and P56 were clearly observed (Figure 3A3 and B3). The RGCs were observed in the en face images (Figure 3A4 and B4). For the P17 mouse, the RGCs were located in the HRL, thus, the individual RGCs were clearly observed. For the P56 mouse, the RGCs were closely packed with NFL and IPL, and the contour of RGCs was not clear.

4. Discussion

In summary, longitudinal OCT of postnatal retinal development has been demonstrated in mice from P14 to P56. Quantitative OCT analysis revealed distinct outer and inner retinal layer changes, corresponding to eye development. An HRL between the NFL and IPL was observed in developing eyes and gradually disappeared with aging. The fine structure development of inner retina layers was analyzed via frame registration and super averaging.

Three possible factors could contribute to the retina thickness change after the eye-opening. First, the eyeball diameter increase [27], causing a general thinning effect, affecting all the retinal layers. Second, cell death during retina development [28], also causes a thinning effect, affecting a few layers. Third, the retinal structure modification [29], causing a thinning or a thickening effect, affecting a few layers. The thickness change of an individual retinal layer can be the combination of all these three effects. As the eyeball expansion affects all retinal layers, the other two factors will be discussed in detail below.

The NFL thickness decreased from P14 to P21 days and become stable after P21 days (Figure 2D1). The change could be explained by the combination of eyeball expansion and retinal structure modification. The RGC population remains stable during the development after eye-opening, therefore, the total number of the axon is stable [28,30]. However, right after eye-opening until postnatal 3 weeks, there is a maximum rate of nerve fiber growth and myelination [31]. It has been reported that, during this period, the number of myelinated nerve fibers, as well as the nerve fiber diameter increase [32], which is considered to be dependent on the environment light stimulation [33]. The never fiber modification causes NFL thickness increase.

The IPL thickness remained stable (Figure 2D1) from P14 to P56 days. The observation could be explained by the combination of eyeball expansion, cell death, and retinal structure modification. IPL is composed of the dendrite and synapse connections between RGCs, bipolar cells, and amacrine cells. After eye-opening, the population of bipolar cells keeps decreasing until P19 days, and the population of amacrine cells also slightly decreases [28]. The apoptosis of these cells causes IPL thickness to decrease. However, during postnatal development, the dendritic field size of RGCs keeps increasing until 3 weeks after birth [5]. The density of both ribbons and conventional synapses in the IPL continuously increases after eye-opening and reaches the peak level by around the age of P21 [8]. This dendritic refinement causes IPL to thicken.

The INL thickness decreased after eye-opening (Figure 2D1) until P28 days. The change could be explained by eyeball expansion and cell death. INL is composed of nuclei of bipolar cells, horizontal cells, and amacrine cells. The layer thickness is only related to the population of the cells. After eye-opening, the population of the horizontal cell remained stable, the population of amacrine cells show a slight decrease, and the population of bipolar cells shows a decrease until P19 [28]. The apoptosis of bipolar cells and amacrine cells causes INL thinning.

Similar to INL, the ONL thickness also decreased after eye-opening (Figure 2D2) until p28 days. The change could be explained by eyeball expansion, and cell death. ONL is composed of the nuclei of retinal photoreceptors. The population of photoreceptors keeps decreasing until P24 days [28], which could cause ONL thinning.

The ELM-RPE thickness increased after eye-opening (Figure 2D2) until P28 days. ELM to RPE layer is composed of photoreceptor inner segment, outer segment, and RPE layers. The change could be explained by the combination of eyeball expansion, cell death, and photoreceptor inner and outer segment elongation. The population of photoreceptors keeps decreasing until P24 days, which could cause this layer thinning. However, the photoreceptor inner segmentation and outer segmentation both expand significantly [29], which causes this layer to thicken.

To the best of our knowledge, the HRL between NFL and IPL in the OCT B-scans of mouse retina was not reported before. For human OCT images, the hyporeflective layer between NFL and IPL is the ganglion cell layer (GCL). However, for mouse retina, most

studies considered that the RGCs are buried in NFL or IPL. As the intensity of RGCs is much weaker than axons, dendrites, and synapses in NFL and IPL, they are hard to identify in the OCT image [24]. Therefore, for mouse retina segmentation, some people consider the RGCs are included in NFL and call it NFL-GCL complex [34-37]; some people consider the RGCs are included in IPL and call it GCL-IPL layer [38,39]; some people simply use NFL or GCL to denote the layer that above IPL [40,41]. From the *en face* image (Figure 3A3 & 4B3) at the location of HRL, we could see individual RGC somas. By comparing en face images of P17 and P56 mice, we can see that the RGCs of P17 were "cleaner" and the RGCs of P56 are collocated with nerve fibers and neuron dendrites and synapses. Considering the IPL and nerve fiber refinement after the eye-opening, we speculate that this hyporeflective band between GCL and IPL is RGCs. The actual mechanism of the HRL vanishing is not well understood. We have two hypotheses. First, during the refinement of the IPL, the RGCs are well surrounded by the neuron dendrites of bipolar cells, amacrine cells, and RGCs, and thus to reduce the difference of light property in neigboring regions. The other hypothesis is that, during the refinement of the nerve fiber, the RGCs are well packed into the NFL layer, and thus reducing the difference of light property in neighboring regions. In either way, the HRL of RGCs will vanish because of buried in other hyperreflective tissues. An immunofluorescent study could help to test these hypotheses. This immunofluorescent study will not only help to explain the vanishing of HRL but also help to identify the correlation between the retinal OCT image and the anatomic correlate.

The observation of the morphological change of retinal inner layers, such as NFL and IPL, during the retinal postnatal development, is consistent with the observation of IPL modification after eye-opening [8], RGC dendritic refinement [4-6], and nerve fiber growth [32]. The fine structure is hard to observe with OCT, however, with super averaging processing after frame registration, the nerve fibers, individual RGCs, and stratification of IPL could be observed [22-24]. In a previous study, the whole frame registration was executed all by ImageJ. A few hours are needed to finish the frame registration of 150 OCT volumes which contain 512 A-scans times 512 B-scans in each volume. In our approach, the registration information is computed by ImageJ, however, the volume image data transformation is executed by MATLAB. Due to the good performance of 3D matrix computation capability and the parallel computing, the total time coasted by frame registration was within 30 min for 200 volumes which contain 500 A-scans times 500 B-scans in each.

5. Conclusion

In vivo OCT provides a feasible solution for longitudinal monitoring of postnatal retinal development. Quantitative OCT analysis revealed distinct outer and inner retinal layer changes, corresponding to eye development. An HRL between the NFL and IPL was observed in developing eyes and gradually disappeared with aging. The fine structure development of the inner retina was analyzed via frame registration and super averaging. These approaches can be powerful tool for retina development and ROP studies.

Author Contributions:

Conceptualization, Guangying Ma and Xincheng Yao; Data curation, Guangying Ma and Jie Ding; Funding acquisition, Xincheng Yao; Supervision, Xincheng Yao; Visualization, Guangying Ma; Writing – original draft, Guangying Ma; Writing – review & editing, Tae-Hoon Kim and Xincheng Yao.

Funding: National Eye Institute: P30 EY001792, R01 EY030101, R01 EY023522, R01EY029673, R01 EY030842, R44 EY028786; Richard and Loan Hill endowment; unrestricted grant from Research to Prevent Blindness.

Institutional Review Board Statement: Not applicable.

Informed Consent Statement: Not applicable.
Data Availability Statement: The data presented in this study are available on request from the corresponding author.

Conflicts of Interest: None

References

1. Morgan, J.; Wong, R. Development of cell types and synaptic connections in the retina. In *Webvision: the organization of the retina visual system*; 2007.
2. Chan, Y.-C.; Chiao, C.-C. Effect of visual experience on the maturation of ON–OFF direction selective ganglion cells in the rabbit retina. *Vision research* **2008**, *48*, 2466-2475.
3. Tian, N.; Copenhagen, D.R. Visual stimulation is required for refinement of ON and OFF pathways in postnatal retina. *Neuron* **2003**, *39*, 85-96.
4. Tian, N. Development of retinal ganglion cell dendritic structure and synaptic connections. In *Webvision: The Organization of the Retina Visual System*; 2012.
5. Coombs, J.L.; Van Der List, D.; Chalupa, L.M. Morphological properties of mouse retinal ganglion cells during postnatal development. *J Journal of Comparative Neurology* **2007**, *503*, 803-814.
6. Tian, N. Visual experience and maturation of retinal synaptic pathways. *Vision research* **2004**, *44*, 3307-3316.
7. Tian, N.; Copenhagen, D.R. Visual stimulation is required for refinement of ON and OFF pathways in postnatal retina. *Neuron* **2003**, *39*, 85-96.
8. Fisher, L.J. Development of synaptic arrays in the inner plexiform layer of neonatal mouse retina. *Journal of Comparative Neurology* **1979**, *187*, 359-372.
9. Koehler, C.L.; Akimov, N.P.; Rentería, R.C. Receptive field center size decreases and firing properties mature in ON and OFF retinal ganglion cells after eye opening in the mouse. *Journal of neurophysiology* **2011**, *106*, 895-904.
10. Drexler, W.; Fujimoto, J.G. *Optical coherence tomography: technology and applications*; Springer Science & Business Media: 2008.
11. Hariri, S.; Moayed, A.A.; Choh, V.; Bizheva, K. In vivo assessment of thickness and reflectivity in a rat outer retinal degeneration model with ultrahigh resolution optical coherence tomography. *Investigative ophthalmology visual science* **2012**, *53*, 1982-1989.
12. Nivison-Smith, L.; Wang, H.; Assaad, N.; Kalloniatis, M. Retinal Thickness Changes throughout the Natural History of Drusen in Age-related Macular Degeneration. *Optometry and Vision Science* **2018**, *95*, 648-655, doi:10.1097/opx.0000000000001256.
13. Kim, T.-H.; Son, T.; Klatt, D.; Yao, X. Concurrent OCT and OCT angiography of retinal neurovascular degeneration in the 5XFAD Alzheimer's disease mice. *Neurophotonics* **2021**, *8*, 035002.
14. Chauhan, B.C.; Stevens, K.T.; Levesque, J.M.; Nuschke, A.C.; Sharpe, G.P.; O'Leary, N.; Archibald, M.L.; Wang, X. Longitudinal in vivo imaging of retinal ganglion cells and retinal thickness changes following optic nerve injury in mice. *PloS one* **2012**, *7*, e40352.
15. Zeimer, R.; Asrani, S.; Zou, S.; Quigley, H.; Jampel, H. Quantitative detection of glaucomatous damage at the posterior pole by retinal thickness mapping: a pilot study. *Ophthalmology* **1998**, *105*, 224-231.
16. Maldonado, R.S.; O'Connell, R.V.; Sarin, N.; Freedman, S.F.; Wallace, D.K.; Cotten, C.M.; Winter, K.P.; Stinnett, S.; Chiu, S.J.; Izatt, J.A. Dynamics of human foveal development after premature birth. *Ophthalmology* **2011**, *118*, 2315-2325.
17. Kim, T.H.; Son, T.; Yao, X. Feature article: Functional OCT angiography reveals early physiological dysfunction of hyaloid vasculature in developing mouse eye. *Exp Biol Med (Maywood)* **2019**, *244*, 819-823, doi:10.1177/1535370219850787.
18. Kim, T.H.; Son, T.; Le, D.; Yao, X. Longitudinal OCT and OCTA monitoring reveals accelerated regression of hyaloid vessels in retinal degeneration 10 (rd10) mice. *Sci Rep* **2019**, *9*, 16685, doi:10.1038/s41598-019-53082-9.

19. Kim, T.H.; Son, T.; Lu, Y.; Alam, M.; Yao, X. Comparative Optical Coherence Tomography Angiography of Wild-Type and rd10 Mouse Retinas. *Transl Vis Sci Technol* **2018**, *7*, 42, doi:10.1167/tvst.7.6.42.
20. Smith, L.E. Pathogenesis of retinopathy of prematurity. *Growth hormone IGF research* **2004**, *14*, 140-144.
21. Morita, M.; Ohneda, O.; Yamashita, T.; Takahashi, S.; Suzuki, N.; Nakajima, O.; Kawauchi, S.; Ema, M.; Shibahara, S.; Udono, T. HLF/HIF‐2α is a key factor in retinopathy of prematurity in association with erythropoietin. *The EMBO journal* **2003**, *22*, 1134-1146.
22. Pi, S.; Hormel, T.T.; Wei, X.; Cepurna, W.; Morrison, J.C.; Jia, Y. Imaging retinal structures at cellular-level resolution by visible-light optical coherence tomography. *Optics letters* **2020**, *45*, 2107-2110.
23. Liu, Z.; Kurokawa, K.; Zhang, F.; Lee, J.J.; Miller, D.T. Imaging and quantifying ganglion cells and other transparent neurons in the living human retina. *Proceedings of the National Academy of Sciences* **2017**, *114*, 12803-12808.
24. Zhang, P.; Miller, E.B.; Manna, S.K.; Meleppat, R.K.; Pugh, E.N.; Zawadzki, R. Temporal speckle-averaging of optical coherence tomography volumes for in-vivo cellular resolution neuronal and vascular retinal imaging. *Neurophotonics* **2019**, *6*, 041105.
25. Ma, G.; Son, T.; Kim, T.H.; Yao, X. In vivo optoretinography of phototransduction activation and energy metabolism in retinal photoreceptors. *Journal of Biophotonics* **2021**, *14*, e202000462.
26. Son, T.; Alam, M.; Toslak, D.; Wang, B.; Lu, Y.; Yao, X. Functional optical coherence tomography of neurovascular coupling interactions in the retina. *Journal of biophotonics* **2018**, *11*, e201800089.
27. Tkatchenko, T.V.; Shen, Y.; Tkatchenko, A.V. Analysis of postnatal eye development in the mouse with high-resolution small animal magnetic resonance imaging. *Investigative ophthalmology visual science* **2010**, *51*, 21-27.
28. Young, R.W. Cell death during differentiation of the retina in the mouse. *Journal of Comparative Neurology* **1984**, *229*, 362-373.
29. Caley, D.W.; Johnson, C.; Liebelt, R.A. The postnatal development of the retina in the normal and rodless CBA mouse: a light and electron microscopic study. *American Journal of Anatomy* **1972**, *133*, 179-211.
30. Farah, M.H.; Easter Jr, S.S. Cell birth and death in the mouse retinal ganglion cell layer. *Journal of Comparative Neurology* **2005**, *489*, 120-134.
31. Dangata, Y.; Findlater, G.; Kaufman, M. Postnatal development of the optic nerve in (C57BL x CBA) F1 hybrid mice: general changes in morphometric parameters. *Journal of anatomy* **1996**, *189*, 117.
32. Gyllensten, L.; Malmfors, T.r. Myelinization of the optic nerve and its dependence on visual function—a quantitative investigation in mice. *Embryol Exp Morphol.* **1963**.
33. Gyllensten, L.; Malmfors, T.; Norrlin‐Grettve, M.L. Developmental and functional alterations in the fiber composition of the optic nerve in visually deprived mice. *Journal of Comparative Neurology* **1966**, *128*, 413-418.
34. Antony, B.J.; Jeong, W.; Abramoff, M.D.; Vance, J.; Sohn, E.H.; Garvin, M.K. Automated 3D segmentation of intraretinal surfaces in SD-OCT volumes in normal and diabetic mice. *Translational vision science technology* **2014**, *3*, 8-8.
35. Ruggeri, M.; Wehbe, H.; Jiao, S.; Gregori, G.; Jockovich, M.E.; Hackam, A.; Duan, Y.; Puliafito, C.A. In vivo three-dimensional high-resolution imaging of rodent retina with spectral-domain optical coherence tomography. *Investigative ophthalmology visual science* **2007**, *48*, 1808-1814.
36. Zhang, P.; Zam, A.; Jian, Y.; Wang, X.; Li, Y.; Lam, K.S.; Burns, M.E.; Sarunic, M.V.; Pugh Jr, E.N.; Zawadzki, R.J. In vivo wide-field multispectral scanning laser ophthalmoscopy–optical coherence tomography mouse retinal imager: longitudinal imaging of ganglion cells, microglia, and Müller glia, and mapping of the mouse retinal and choroidal vasculature. *Journal of biomedical optics* **2015**, *20*, 126005.
37. Harper, D.J.; Augustin, M.; Lichtenegger, A.; Gesperger, J.; Himmel, T.; Muck, M.; Merkle, C.W.; Eugui, P.; Kummer, S.; Woehrer, A. Retinal analysis of a mouse model of Alzheimer's disease with multicontrast optical coherence tomography. *Neurophotonics* **2020**, *7*, 015006.

38. Dysli, C.; Enzmann, V.; Sznitman, R.; Zinkernagel, M.S. Quantitative analysis of mouse retinal layers using automated segmentation of spectral domain optical coherence tomography images. *Translational vision science technology* **2015**, *4*, 9-9.
39. Srinivasan, P.P.; Heflin, S.J.; Izatt, J.A.; Arshavsky, V.Y.; Farsiu, S. Automatic segmentation of up to ten layer boundaries in SD-OCT images of the mouse retina with and without missing layers due to pathology. *Biomedical optics express* **2014**, *5*, 348-365.
40. Pennesi, M.E.; Michaels, K.V.; Magee, S.S.; Maricle, A.; Davin, S.P.; Garg, A.K.; Gale, M.J.; Tu, D.C.; Wen, Y.; Erker, L.R. Long-term characterization of retinal degeneration in rd1 and rd10 mice using spectral domain optical coherence tomography. *Investigative ophthalmology visual science* **2012**, *53*, 4644-4656.
41. Hanna, J.; Yücel, Y.H.; Zhou, X.; Mathieu, E.; Paczka-Giorgi, L.A.; Gupta, N. Progressive loss of retinal blood vessels in a live model of retinitis pigmentosa. *Canadian Journal of Ophthalmology* **2018**, *53*, 391-401.